Article type: Full Paper

3D Bioprinting of Developmentally Inspired Templates for Whole Bone Organ Engineering

Andrew C. Daly, Gráinne M. Cunniffe, Binulal N. Sathy,   Oju Jeon,   Eben Alsberg, , Daniel J. Kelly [*]

Mr. Andrew C. Daly, Dr. Gráinne M. Cunniffe, Dr. Binulal N. Sathy
Trinity Centre for Bioengineering & Department of Mechanical & Manufacturing Engineering
Trinity College Dublin, The University of Dublin, Dublin 2, (Ireland)

Dr. Oju Jeon, Prof. Eben Alsberg
Departments of Biomedical Engineering and Orthopedic Surgery, and the National Centre for Regenerative Medicine, Case Western Reserve University, Cleveland, Ohio, (USA)

[*]   Prof. Daniel J. Kelly (Corresponding-Author)
Trinity Centre for Bioengineering & Department of Mechanical & Manufacturing Engineering,
Department of Mechanical & Manufacturing Engineering,
Trinity College Dublin, The University of Dublin, Dublin 2, (Ireland)
E-mail: kellyd9@tcd.ie

1

Abstract

The ability to print defined patterns of cells and extracellular-matrix components in three dimensions has enabled the engineering of simple biological tissues, however bioprinting functional solid organs is beyond the capabilities of current biofabrication technologies. An alternative approach would be to bioprint the developmental precursor to an adult organ, using this engineered rudiment as a template for subsequent organogenesis *in vivo*. Here we demonstrate that developmentally inspired hypertrophic cartilage templates can be engineered *in vitro* using stem cells within a supporting gamma-irradiated alginate bioink incorporating Arg-Gly-Asp (RGD) adhesion peptides. Furthermore, these soft tissue templates can be reinforced with a network of printed polycaprolactone fibres, resulting in a ~350 fold increase in construct compressive modulus providing the necessary stiffness to implant such immature cartilaginous rudiments into load bearing locations. As a proof-of-principal, multiple-tool biofabrication was used to engineer a mechanically reinforced cartilaginous template mimicking the geometry of a vertebral body, which *in vivo* supported the development of a vascularized bone organ containing trabecular-like endochondral bone with a supporting marrow structure. Such developmental engineering approaches could be applied to the biofabrication of other solid organs by bioprinting pre-cursors that have the capacity to mature into their adult counterparts over time *in vivo*.

1. Introduction

Bioprinting is an emerging tool to spatially control the deposition of biomaterials, biomolecules and/or cells in predefined three dimensional (3D) patterns [1–3]. This technology has already been used to engineer constructs that mimic aspects of the anatomical and structural complexity of relatively thin tissues and hollow tubes such as skin [4], blood vessels [5] and articular cartilage [6]. However reproducing the complex cellular and extra-cellular micro-organisation of an entire solid organ is well beyond the capabilities of currently available bioprinting technologies. An alternative approach would be to bioprint the developmental precursor of a more complex organ, as the structure and composition of such rudiments are typically less complex than their adult counterparts. If such developmentally inspired bioprinted implants can be provided with adequate mechanical support to survive and function within the adult body, they may provide a template to instruct organogenesis *in vivo*. Such a developmental engineering approach would add a new dimension to the traditional bioprinting paradigm by providing organ pre-cursors with the capacity to mature into their more complex adult counterparts over time *in vivo*.

During skeletogenesis the long bones of the body are formed by endochondral ossification, whereby chondrocytes within the developing limb bud undergo a coordinated sequence of proliferation and hypertrophy, providing a growing template for bone formation [7,8]. Cartilage canals within this cartilaginous precursor act as conduits for vascular invasion to enable its conversion into bone [9]. It has been demonstrated that cartilaginous templates generated *in vitro* using adult mesenchymal stem cells (MSCs) are vascularised and form bone following implantation [10–13], suggesting that such engineered tissues could be used for the reconstruction of large bone defects. A central challenge with the translation of such developmentally inspired engineering strategies is ensuring that these immature soft tissues, which are designed to function in the relatively low load bearing environment of the developing limb, are provided with the necessary mechanical support to execute their function in the adult body.

In this work we utilize 3D bioprinting to engineer anatomically accurate, mechanically reinforced, hypertrophic cartilage templates which develop over time *in vivo* to give rise to whole bone organs. A range of hydrogel bioinks were first compared for their capacity to support chondrogenesis of MSCs *in vitro* and endochondral bone formation *in vivo*. An array of micro-channels inspired by the cartilage canal network that form during long bone development were introduced into the bioprinted constructs to support their vascularisation and conversion into endochondral bone [14]. These engineered hypertrophic cartilaginous templates were then mechanically reinforced with a network of printed polycaprolactone (PCL) microfibers. Finally, we demonstrate the power of this developmental 3D bioprinting approach by using multi-tool biofabrication to engineer developmentally inspired templates mimicking the geometry and bulk mechanical properties of a vertebral body, which over time *in vivo* matured into a vascularized bone organ.

2. Results

2.1. Printable Hydrogels for Endochondral Bone Tissue Engineering

Realising the objectives of this study first required the identification of a hydrogel *bioink* that was both compatible with 3D bioprinting and also capable of supporting robust chondrogenesis *in vitro* and endochondral bone formation *in vivo*. Three hydrogels compatible with 3D bioprinting, namely a gamma-irradiated alginate incorporating Arg-Gly-Asp (RGD) specific adhesion peptides (RGD-γ alginate; previously developed to support bone regeneration [15–17]), a commercially available poly (ethylene glycol) methacrylate (PEGMA) based hydrogel designed specifically for 3D Bioprinting (marketed as BioINK™) and finally Gelatin methacrylamide (GelMA) [18], were first compared for their capacity to support chondrogenesis of bone marrow derived MSCs **(Figure 1a)**. MSCs were encapsulated in each of the hydrogels and cultured in chondrogenic conditions for a period of 4 weeks. To compare the printability of each hydrogel cell laden filaments were deposited onto a glass slide using a 25G needle (260μm) and the average filament diameter was measured **(Figure S1 c).**

Histological and immunohistochemical staining at the end of the 4 week *in vitro* culture period demonstrated that each hydrogel supported differing degrees of chondrogenesis **(Figure. 1b).** RGD-γ alginate supported stronger chondrogenic differentiation, with engineered tissues staining intensely for sGAG and collagen type II **(Figure 1b i, vii)**. In contrast, the GelMA and PEGMA hydrogels supported lower levels of sGAG and collagen type II staining **(Figure 1b ii, iii, viii, ix)**. sGAG synthesis (sGAG/DNA) was significantly lower in the GelMA constructs compared to all other hydrogels **(Figure 1b xviii, xix)**. Cells encapsulated in RGD-γ alginate hydrogels appeared larger in volume with more well developed lacunae **(Figure 1b iv)**. Negligible collagen type X, a marker of chondrocyte hypertrophy, was found in PEGMA and GelMA, with slightly higher staining noted in

peri-cellular regions of the RGD-γ alginate hydrogel **(Figure 1b iv-vi)**. Acellular staining for sGAG and day 0 sGAG/DNA values for each biopolymer are also provided in **(Figure S1 a-c).**

Next the chondrogenically primed hydrogels were implanted subcutaneously into nude mice to compare their capacity to support the conversion of an engineered cartilage template into bone *in vivo*. H&E staining, as well as µCT analysis, were used to assess spatial bone formation. Small pockets of bone developed within peripheral regions of the PEGMA templates, while bone formation (although still somewhat peripheral) was more diffuse within the RGD-γ alginate and GelMA templates **(Figure 2, a, e, i)**. µCT analysis confirmed that each hydrogel supported the development of a mineralised envelope **(Figure 2, m-o)**. GelMA and RGD-γ alginate supported higher levels of mineralisation within core regions compared to the other templates **(Figure 2, p-r)**, with quantification of the µCT reconstructions revealing RGD-γ alginate hydrogels supported the highest absolute levels of mineral accumulation **(Figure 2 s)**. Collagen type X and collagen type I staining, two markers of chondrocyte hypertrophy and endochondral ossification, were strongest in the modified RGD-γ alginate hydrogel **(Figure 2 c, d, g, h, k, l)**. The levels of sGAG within each of the hydrogels dropped over the 6 week *in vivo* period while the collagen levels increased in the alginate and PEGMA hydrogels (Figure S2 a, b). As RGD-γ alginate appeared to best support the development of endochondral bone *in vivo*, it was chosen for use as a bioink for subsequent bioprinting of developmentally inspired hypertrophic cartilage rudiments.

2.2. Bioprinting of Mechanically Reinforced Cartilage Rudiments for Endochondral Bone Formation

After determining the optimum bioink (RGD-γ alginate) to engineer endochondral bone *in vivo,* we next sought to engineer a mechanically reinforced soft tissue templates suitable for load bearing applications by combining 3D printed PCL scaffolds (fibre diameter 437 ± 64 µm, porosity 67%) with an MSC laden bioink **(Figure 3a)**. Reinforcement with PCL led to a dramatic increase in the compressive modulus (*3.867± 0.2187 kPa vs. 1402 ± 157.8 kPa*; Figure 3b), approaching that

found for trabecular bone which can range from 1 MPa upwards depending on location[19]. To determine if incorporating a slowly degrading PCL phase into the MSC laden bioink influenced endochondral bone formation *in vivo*, these composite constructs were chondrogenically primed *in vitro* and then implanted subcutaneously in nude mice. In addition, we explored whether altering the construct architecture through incorporation of micro-channels into the composite bioink/PCL grafts would accelerate vascularisation and bone formation following implantation *in vivo (bioink/PCL + Channels)* [12]. All constructs (bioink, bioink/PCL & bioink/PCL + Channels) were chondrogenically primed *in vitro* for 4 weeks **(Figure S3 a, b, c)** and implanted subcutaneously for 4 & 12 weeks to compare their capacity to support endochondral bone formation *in vivo*.

After 4 weeks *in vivo*, all constructs were stained to evaluate the presence of sGAG, collagen type II, collagen type I & collagen type X. Reinforcement with PCL appeared to support the development of a more hypertrophic cartilaginous template, with higher levels of collagen type X accumulation compared to the PCL-free bioink **(Figure 3c, iv-vi)**. More intense staining for collagen type I was also found in the PCL-composites, again indicative of more advanced progression along the endochondral pathway **(Figure 3c x-xii)**.

After 12 weeks *in vivo*, histomorphometric quantification and µCT analysis demonstrated that both composite bioinks supported significantly higher levels of bone formation **(Figure 4 a-i, n)**. H&E staining also revealed areas of red blood cell activity within the composite bioink/PCL constructs indicating vascularisation of the grafts **(Figure 4 j-l)**, with significantly higher numbers of vessels found in the composite groups at both 4 and 12 weeks compared to the bioink only controls **(Figure 4m)**. µCT analysis confirmed significantly higher levels of mineralisation within the composite groups compared to the bioink control **(Figure 4o)**. The bone forming capacity of these printed constructs was also scalable, as geometrically larger templates were also found to vascularise and mineralise at similar levels to smaller engineered tissues **(Figure S4)**.

2.3. Bioprinting of Developmentally Inspired Cartilage Rudiments for Whole Bone Organ Engineering

We next explored the possibility of bioprinting a hypertrophic cartilage rudiment that could act as a template for the formation of a whole bone organ *in vivo*. A model of a human vertebrae was scanned using a PICZA 3D laser scanner and converted to stereolithographic (STL) format. Next the STL file was converted to g-code to control the deposition of PCL and MSC laden bioink filaments. For this phase of the study, rather than infusing the MSC laden bioink into a pre-printed PCL network, the constructs were 3D bioprinted by co-depositing bioink filaments alongside PCL filaments in a layer by layer fashion using multiple-tool biofabrication to build a composite vertebrae structure **(Figure 5a)**. By controlling the placement of the bioink within every second PCL fibre spacing it was possible to introduce a network of interconnected bioink-free channels within the PCL construct **(Figure 5b)**. Live-dead staining demonstrated the cells remained viable within the bioink network post-printing **(Figure 5c)**. Next the constructs were chondrogenically primed *in vitro* as described previously and implanted subcutaneously for 12 weeks to assess whether this bioprinting strategy could be used to engineer a whole bone organ.

12 weeks post-implantation the bioprinted vertebrae was extensively vascularised and mineralised **(Figure 6a)**. μCT analysis demonstrated that $24.6 \pm 4.8\%$ of the bioprinted construct consisted of bone tissue **(Figure 6b)**. H&E staining confirmed the presence of bone throughout the depth of the vertebrae **(Figure 6 c, d, f, h)**. Goldners trichrome staining demonstrated the presence of immature osteoid tissue surrounding networks of hypertrophic chondrocytes **(Figure 6 e, g)**. Areas of red blood cell activity indicated vascular networks were present in the constructs (Figure 6j). In addition there was evidence of bone marrow like tissue surrounded by bony trabeculae with osteocytes embedded in their lacunae **(Figure 6l)**. Intense staining for collagen type X indicated bone formation occurred via an endochondral pathway through remodelling of the hypertrophic cartilage template **(Figure 6 i, k)**. Near comparable levels of mineralisation were found when the bioink was

switched from RGD-γ alginate to GelMA, demonstrating that mineralisation was not due to calcification of the RGD-γ alginate material itself **(Figure S5 c, d, e)**. In addition, no mineralisation or bone were found in empty PCL controls where the constructs were filled with fibrous tissue **(Figure S5 b, d)**.

3. Discussion

In this study we demonstrate the feasibility of engineering an entire bone organ using a novel 3D bioprinting strategy. Using multiple-tool biofabrication, we were able to engineer an organ precursor *in vitro* which subsequently provided a template for the formation of its more complex adult counterpart *in vivo*. Having identified a suitable bioink to tissue engineer a cartilaginous rudiment, we then demonstrated that is was possible to mechanically reinforce this template using a network of printed PCL microfibers, resulting in composite constructs with a compressive modulus approaching that of cancellous bone. Finally, we leveraged the capacity of multiple-tool biofabrication to engineer a reinforced soft tissue template mimicking the geometry of a whole vertebrae. After chondrogenic priming, this construct was found to support the development of a functional bone organ *in vivo*.

The RGD-γ alginate bioink was found to support more robust chondrogenesis of MSCs *in vitro* and enhanced levels of endochondral bone formation *in vivo* compared to both the PEGMA and GelMA based bioinks. It is well established that alginate hydrogels can support robust chondrogenesis [20,21], with the incorporation of RGD peptides having previously been shown to lead to enhanced osteogenesis when this biomaterial is used for bone tissue engineering applications [15,17]. Furthermore, we chose to use a gamma-irradiated alginate as the relatively slow degradation rate of this hydrogel in its non-modified form has previously been shown to impede endochondral bone regeneration [22]. The alginate bioink was physically cross-linked using $CaCl_2$ whereas the PEGMA and GelMA bioinks were both chemically cross linked using UV light. This could also contribute to the higher levels of endochondral bone formed in the alginate bioink as chemical cross links typically degrade

slower. Furthermore, since both PEGMA and GelMA supported lower levels of chondrogenic differentiation *in vitro*, a lower number of MSCs likely reached the terminal hypertrophic phenotype *in vivo*, potentially also contributing to the lower levels of endochondral bone generated within these hydrogels. The higher levels of collagen type X staining found in the alginate hydrogel after 6 weeks of *in vivo* implantation support this hypothesis **(Figure 2 d, h, l)**.

It was possible to reinforce the MSC laden bioink with a network of PCL micro-fibres, thereby providing a level of mechanical functionality compatible with implanting such organ rudiments into load bearing locations *in vivo*. It should be clarified that no attempt was made to chemically cross-link the hydrogel bioink to the PCL fibres. This may be a potential limitation at higher strains and future work will explore improving the integrity of the interface through covalent attachment of the hydrogel to the PCL filaments [23]. Importantly, the capacity of these constructs to support endochondral bone formation was not compromised at the expense of the added mechanical functionality associated with the integration of the PCL micro-fibres. The RGD-γ alginate bioink within the PCL composites appeared to degrade at an accelerated rate compared to the solid bioink controls, likely due to the increased surface to volume ratio of the reinforced bioink. This at least partially explains the greater levels of host cell invasion and vascularisation throughout the composite constructs, which in turn can further accelerate degradation as host derived cells are known to play a key role in remodelling and removal of biomaterials [24] . In agreement with previous studies, bone formation occurred within regions of the construct where the RGD-γ alginate bioink had broken down providing space for vascularization and new tissue formation [21,25]. Increases in oxygen availability associated with enhanced vascularization will in turn accelerate hypertrophy of the implanted grafts [26]. In fact, the capacity of the cartilaginous constructs to generate endochondral bone was improved by the incorporation of PCL. Although there was a trend toward higher levels of vascularisation in the channelled constructs, no significant increase in mineralization was found with the incorporation of these micro-channels as has been previously reported [12]. This may be due to the fact that the

addition of PCL alone increased the surface to volume ratio of the RGD-γ alginate bioink as described above, hence no further benefits accrued through the incorporation of micro-channels.

In this study, we used PCL to provide structural support to the construct and RGD-γ-Alginate as a bioink to enable the printing of MSCs and to provide an environment conductive to chondrogenesis. The degradation rate of the PCL (MW above 45,000 g/mol) *in vivo* is slow, typically 24-30 months before the polymer breaks down into lower molecular weight fragments [27,28] First the polymer surface is slowly degraded by hydrolytic cleavage at the surface resulting in thinning of the fibres followed by a more rapid phase of bulk degradation when water penetrates the entire polymer matrix. This slow degradation would be beneficial in high load bearing bone defects where long term support is required before the tissue can fully repair. The alginate hydrogel (MW 58,000 g/mol) will degrade more rapidly than the PCL polymer. Alginate hydrogels dissolve at neutral pH upon losing divalent cross linking cations to surrounding body fluids. Here we used a low molecular weight alginate hydrogel produced by irradiating (5mrad) the polymer as it has been shown that lower molecular weight gels are cleared more rapidly *in vivo* [16]. It has recently been shown in a rat femoral defect model that 60-70% of the polymer degrades away from the site of bone formation after 12 weeks of implantation[29]. Higher levels of irradiation (8mrad) can be utilised to produce alginate hydrogels that will lose 90% of their mass 2 weeks after implantation [16].

Engineering of solid organs is the perhaps the ultimate aim of regenerative medicine, but remains elusive as current biofabrication strategies cannot recapitulate such intricate 3D structures [30]. The approach developed here facilitates the positioning of multiple materials and cells within 3D structures, enabling the engineering of pre-cursors to more complex organs. The approach could also be adapted to other biofabrication methods such as inkjet printing and electrospinning where cellular and extra cellular material can be arranged in complex patterns [31]. Future work will look at recapitulating biomolecule gradients that occur during skeletal developmental processes using bioprinted patterns of plasmid DNA encoding for vascular, chondrogenic and osteogenic factors such as VEGF, PDGF, TGF-β3 and BMP-2 [32–35]. We will also explore the spatial and temporal control of

11

these and other factors [3,36] to help engineer the micro-environment of developing bones. Another major challenge in tissue engineering is integrating larger solid tissues with the surrounding host vasculature post implantation to maintain cell viability [37]. Here the vertebrae structures were well vascularised post-implantation, indicating that the engineered cartilage rudiments are capable of recruiting host vessels *in vivo* to support both implanted and recruited cells within the implant.

4. Conclusion

In conclusion, this study presents a novel biofabrication strategy for engineering whole bone organs by bioprinting developmentally inspired templates with the capacity to undergo endochondral ossification over time following implantation. By printing a customized MSC laden bioink alongside a network of reinforcing PCL microfibers, it was possible to engineer templates where biological and mechanical functionality are decoupled. The additional mechanical functionality provided by the co-deposition of a PCL network during the printing process did not compromise the capacity of the implant to support endochondral bone formation, but should enable such 'developmentally immature' constructs to be implanted into challenging load-bearing environments. Finally, it was possible to engineer a vertebral body incorporating a functional vasculature, trabecular-like bone and a supporting marrow cavity using the approach. Taken together, these results demonstrate the promise of the proposed 3D bioprinting strategy for the engineering of whole bones for orthopaedic and craniofacial medicine. This concept of bioprinting developmental precursors could also be used to engineer other complex solid organs.

5. Experimental Section

Isolation and expansion of MSCs:

Bone marrow derived MSCs were isolated from the femoral shaft of 4 month old pigs and expanded as previously described [38]. Tri-potentiality was confirmed prior to use. Following colony formation, MSCs were trypsinized, counted, seeded at density of 5000 cells cm^2 in 500 cm^2 triple flasks (Thermo Fisher Scientific), supplemented with hgDMEM, 10% v/v FBS, 100 U ml $^{-1}$ penicillin/100 μg ml $^{-1}$ streptomycin, 2.5 μg ml $^{-1}$ amphotericin B and 5 ng ml $^{-1}$ human fibroblastic growth factor-2 (FGF-2; Prospec-Tany TechnoGene Ltd., Israel) and expanded to passage 2. Separate donors were isolated for study 1, 2 & 3.

RGD-γ Alginate and GelMA Synthesis:

Low molecular weight sodium alginate (γ alginate, 58,000 g/mol) was prepared by irradiating sodium alginate (MVG, 259,000 g/mol, Pronova Biopolymers, Oslo, Norway) at a gamma dose of 5 Mrad, as previously described [16]. RGD-modified alginates were prepared by coupling the GGGGRGDSP to the alginate using standard carbodiimide chemistry. Briefly, 10 g alginate was dissolved at 1 w/v % in MES Buffer (0.1 M MES, 0.3 M NaCl and pH 6.5). 274 mg sulfo-NHS (Pierce, Rockford, IL), 484 mg EDC (Sigma), and 100 mg GGGGRGDSP peptide (AIBioTech, Richmond, VA) were then added into alginate solution. The reaction was stopped and the solution was purified and lyophilized as previously described [39]. GelMA was synthesized by reaction of porcine type A gelatin (Sigma Aldrich) with methacrylic anhydride (Sigma Aldrich) at 50 °C for four hours, as previously described [40]. Methacrylic anhydride was added to a 10% solution of gelatin in PBS under constant stirring. To achieve a high degree of functionalization, 0.6 g of methacrylic anhydride was added per gram of gelatin. The functionalized polymer was dialyzed against distilled water for 7 days at 40 °C to remove methacrylic acid and anhydride, freeze-dried and stored at -20 °C until use. NMR was used to confirm functionalisation of the alginate and GelMA hydrogels. PEGMA a polyethylene glycol methacrylamide based hydrogel was purchased from Regen Hu, Switzerland, sold as BioINK™.

Encapsulation of MSCs within alginate, RGD-γ alginate, PEGMA and GelMA Hydrogels:

To cast cylindrical hydrogels (5mm diameter X 3 mm height) RGD-γ alginate (2.45%), PEGMA (concentration undisclosed) and GelMA (10%, Irgacure 2959 0.05%) hydrogels were pipetted into custom developed agarose moulds at a cell density of 20×10^6 MSCs ml $^{-1}$. For fabrication of alginate hydrogels a 4% agarose/50mM CaCl2 mold was cast, and gelation was allowed to occur for 30 min at 37°. Bioink and GelMA constructs were cross-linked by applying UV light (Uvitec, Cambridge UK) for 30 mins (365nM, 180 mW/cm^2). All hydrogels concentrations were chosen for their optimum extrusion characteristics.

3D Bioprinting System:

PCL/bioink scaffolds were fabricated using the 3D Discovery multi-head bioprinting system purchased from Regen Hu, Switzerland. The 3D Discovery was set up to allow for co-printing of two pneumatic driven syringes containing bioinks alongside one fused deposition modeller allowing for deposition of melted polycaprolactone (PCL) (Sigma, Mn 45,000). First the RGD-γ alginate bioink was dissolved at 3.5 wt% and mixed thoroughly with 60mM CaCL$_2$ [41]. A luer lock system was used to mix the alginate and calcium solutions in a 7:3 ratio. To ensure homogeneity the suspension was mixed between syringes 25 times. The solution (2.45 wt% RGD-γ alginate final) was next combined with BMSCs at the end of P2 (20 Million Cells/ml). Next the pre-cross linked MSC laden alginate solution was loaded into the pressure driven piston system and co-printed alongside PCL melted at 60° and 3D Bioprinted (Figure 5A). A pressure of 0.2 MPa and a 25 Gauge needle were used to deposit the bioink/MSC strands. Following this the constructs were immersed in a 50mM CaCl$_2$ solution for 15 mins to fully cross link the alginate bioink. The 3D Discovery was placed in a laminar flow hood to ensure sterility throughout the biofabrication process. For the final study the vertebrae of a human skeleton model was scanned using a PICZA 3D Laser Scanner model LPX-250. 3D computer-aided design software was used to render the scans. Next the scans were converted to g-

code generated using BioCAD™ software (Regen HU, Switzerland) and vertebrae constructs were co-printed as previously described.

Due to difficulties in co-depositing the MSC laden bioink alongside PCL structure in smaller diameter constructs (< 6mm) the constructs used in study 2 were not co-printed. For fabrication of these smaller constructs first a PCL scaffold was deposited with a fibre spacing of 1 mm and placed in a 4% agarose/50mM CaCl2 cylindrical mould. Next the RGD-γ Alginate constructs were fabricated by pipetting passage 2 MSC-laden (20 x 10^6 cells/mL) RGD-γ alginate solution (2.45 wt. %) into the mould around the PCL scaffold and allowing gelation to occur for 15mins (bioink/PCL) (Figure 3a). To form channels a 0.5mm biopsy punch was used to create six channels through the construct (bioink/PCL + channels) (Figure 3a). Channels were introduced at the end of the 4 week *in vitro* culture period prior to implantation.

In vitro culture conditions:

Chondrogenic and hypertrophic culture conditions were applied as previously described [38]. For study one the *in vitro* priming protocol was defined as 4 weeks in chondrogenic conditions, for study 2 & 3 the *in vitro* priming protocol was defined as 3 weeks in chondrogenic conditions followed by one week in hypertrophic conditions. This was to accelerate transition of the cartilage matrix into bone *in vivo* [10,42].

In vivo subcutaneous implantation:

MSC-seeded RGD-γ alginate, PEGMA and GelMA hydrogels (n=9) were implanted subcutaneously into the back of nude mice (Balb/c; Harlan, UK) as previously described [43]. For the second study bioink, bioink/PCL and bioink/PCL channels (n=9) were implanted with 3 samples inserted per pocket. For larger constructs (10mmØ X 6mm height constructs from study 2 (n=3) and the vertebrae from study 3 (n=9)) only two constructs were implanted per animal due to the larger size. For study 1 the constructs were harvested after 6 weeks, for the second study the constructs were harvested after 4&12 weeks and for the third study the vertebrae constructs were harvested after 12 weeks. Mice

were killed by CO2 inhalation and the animal protocol was reviewed and approved by the ethics committee of Trinity College Dublin and the Irish Medicines Board (IMB).

Biochemical analysis:

Sulphated proteoglycan (sGAG) and DNA content were quantified biochemically using the dimethyl methylene blue dye-binding (DMMB) assay and Hoechst Bisbenzimide 33258 dye assay as previously described [26]. To exclude any background absorbance from the individual biopolymers the PH of the DMMB was adjusted to 1.35 and day 0 sGAG values were subtracted from the week 4 values. Total collagen content was determined by measuring the hydroxyproline content using the dimethylaminobenzaldehyde and chloramine T assay and a hydroxyproline to collagen ratio of 1:7.69.

Histological and Immunohistochemical analysis:

Constructs were processed for histological analysis as previously described [21]. The sections were stained with haematoxylin and eosin (H&E) and goldner's trichrome to assess bone formation and aldehyde fuschin/alcian blue to assess sGAG content. Collagen types I, II and X were evaluated using a standard immunohistochemical technique as previously described [12]. Histomorphometric quantification was carried out using Adobe Photoshop® magic wand tool to isolate areas of bone formation on H&E stained sections and then quantified using image J as previously described [44]. The presence of vascular structures were quantified by counting distinct areas of red blood cell activity as a blood vessel. The number of blood vessels across a whole cross section were then counted.

Live/dead confocal microscopy:

Cell viability was assessed after 24 h using a LIVE/DEAD™ viability/cytotoxicity assay kit as previously described [45] . Live dead quantification was carried out using image J.

Microcomputed tomography:

Microcomputed tomography (µCT) scans were performed as previously described [21]. A Gaussian filter (sigma = 0.8, support = 1) was used to suppress noise and a global threshold of 150

corresponding to a density of 254.59 mg hydroxyapatite/cm^3 was applied. A voxel resolution of 12μm was used throughout. The variance of mineralization with depth through the constructs was analysed qualitatively by examining sections at a depth of 25% and 50% from the top of the construct (quarter & mid-section).

Mechanical Characterisation:

Samples were tested in unconfined compression as previously described [46]. Stress tests were performed with a ramp displacement of 1 mm/s until 10% strain. The compressive modulus was taken as the slope of the stress strain curve between 0-10% strain.

Statistical analysis:

Statistical analysis was performed as previously described [47]. Briefly tukey's test for multiple comparisons was used to compare conditions. Significance was accepted at a level of $p \leq 0.05$, with all graphs representing mean ± standard.

Supporting Information

Supporting Information is available from the Wiley Online Library or from the author.

[1]   S. V Murphy, A. Atala, *Nat. Biotechnol.* **2014**, *32*, 773.

[2]   J. Malda, J. Visser, F. P. Melchels, T. Jüngst, W. E. Hennink, W. J. a Dhert, J. Groll, D. W. Hutmacher, *Adv. Mater.* **2013**, *25*, 5011.

[3]   F. Pati, J. Jang, D.-H. Ha, S. Won Kim, J.-W. Rhie, J.-H. Shim, D.-H. Kim, D.-W. Cho, *Nat. Commun.* **2014**, *5*, 3935.

[4]   W. Lee, J. C. Debasitis, V. K. Lee, J. H. Lee, K. Fischer, K. Edminster, J. K. Park, S. S. Yoo, *Biomaterials* **2009**, *30*, 1587.

[5]   R. P. Visconti, V. Kasyanov, C. Gentile, J. Zhang, R. R. Markwald, V. Mironov, *Expert Opin. Biol. Ther.* **2010**, *10*, 409.

[6]   J. Visser, F. P. W. Melchels, J. E. Jeon, E. M. van Bussel, L. S. Kimpton, H. M. Byrne, W. J. a Dhert, P. D. Dalton, D. W. Hutmacher, J. Malda, *Nat. Commun.* **2015**, *6*, 6933.

[7]   a Vortkamp, K. Lee, B. Lanske, G. V Segre, H. M. Kronenberg, C. J. Tabin, *Science* **1996**, *273*, 613.

[8]   E. J. Mackie, Y. a Ahmed, L. Tatarczuch, K.-S. Chen, M. Mirams, *Int. J. Biochem. Cell Biol.* **2008**, *40*, 46.

[9]   M. J. F. Blumer, S. Longato, E. Richter, M. T. Pérez, K. Z. Konakci, H. Fritsch, *J. Anat.* **2005**, *206*, 359.

[10]   C. Scotti, B. Tonnarelli, A. Papadimitropoulos, A. Scherberich, S. Schaeren, A. Schauerte, J. Lopez-Rios, R. Zeller, A. Barbero, I. Martin, *Proc. Natl. Acad. Sci. U. S. A.* **2010**, *107*, 7251.

[11]   J. Visser, D. Gawlitta, K. E. M. Benders, S. M. H. Toma, B. Pouran, P. R. van Weeren, W. J. a. Dhert, J. Malda, *Biomaterials* **2014**, *37*, 174.

[12]   E. J. Sheehy, T. Vinardell, M. E. Toner, C. T. Buckley, D. J. Kelly, *PLoS One* **2014**, *9*, e90716.

[13]   C. Scotti, E. Piccinini, H. Takizawa, A. Todorov, P. Bourgine, A. Papadimitropoulos, A. Barbero, M. G. Manz, I. Martin, *Proc. Natl. Acad. Sci. U. S. A.* **2013**, *110*, 3997.

[14]   M. J. F. Blumer, S. Longato, H. Fritsch, *Ann. Anat. - Anat. Anzeiger* **2008**, *190*, 305.

[15] E. Alsberg, K. W. Anderson, a Albeiruti, R. T. Franceschi, D. J. Mooney, *J. Dent. Res.* **2001**, *80*, 2025.

[16] E. Alsberg, H. J. Kong, Y. Hirano, M. K. Smith, a Albeiruti, D. J. Mooney, *J. Dent. Res.* **2003**, *82*, 903.

[17] E. Alsberg, K. W. Anderson, A. Albeiruti, J. A. Rowley, D. J. Mooney, *PNAS* **2002**, *99*, 12025.

[18] T. Billiet, E. Gevaert, T. De Schryver, M. Cornelissen, P. Dubruel, *Biomaterials* **2014**, *35*, 49.

[19] S. a Goldstein, *J. Biomech.* **1987**, *20*, 1055.

[20] H. a Awad, M. Q. Wickham, H. a Leddy, J. M. Gimble, F. Guilak, *Biomaterials* **2004**, *25*, 3211.

[21] E. J. Sheehy, T. Mesallati, T. Vinardell, D. J. Kelly, *Acta Biomater.* **2014**, *13*, 245.

[22] G. M. Cunniffe, T. Vinardell, E. M. Thompson, a. Daly, a. Matsiko, F. J. O'Brien, D. J. Kelly, *Eur. Polym. J.* **2015**, DOI 10.1016/j.eurpolymj.2015.07.021.

[23] K. W. M. Boere, J. Visser, H. Seyednejad, S. Rahimian, D. Gawlitta, M. J. van Steenbergen, W. J. a Dhert, W. E. Hennink, T. Vermonden, J. Malda, *Acta Biomater.* **2014**, *10*, 2602.

[24] J. M. Anderson, A. Rodriguez, David T. Chang, *Semin Immunol* **2009**, *20*, 86.

[25] C. a Simmons, E. Alsberg, S. Hsiong, W. J. Kim, D. J. Mooney, *Bone* **2004**, *35*, 562.

[26] E. J. Sheehy, D. J. Kelly, C. T. Buckley, *Biochem. Biophys. Res. Commun.* **2012**, *417*, 305.

[27] M. A. Woodruff, D. W. Hutmacher, *Prog. Polym. Sci.* **2010**, *35*, 1217.

[28] H. Sun, L. Mei, C. Song, X. Cui, P. Wang, *Biomaterials* **2006**, *27*, 1735.

[29] L. B. Priddy, O. Chaudhuri, H. Y. Stevens, L. Krishnan, B. a Uhrig, N. J. Willett, R. E. Guldberg, *Acta Biomater.* **2014**, *10*, 4390.

[30] A. Atala, F. K. Kasper, A. G. Mikos, *Sci. Transl. Med.* **2012**, *4*, 160rv12.

[31] A.-V. Do, B. Khorsand, S. M. Geary, A. K. Salem, *Adv. Healthc. Mater.* **2015**, *4*, 1742.

[32] S. Elangovan, B. Khorsand, A. V. Do, L. Hong, A. Dewerth, M. Kormann, R. D. Ross, D.

Rick Sumner, C. Allamargot, A. K. Salem, *J. Control. Release* **2015**, *218*, 22.

[33] S. Elangovan, S. R. D'Mello, L. Hong, R. D. Ross, C. Allamargot, D. V. Dawson, C. M. Stanford, G. K. Johnson, D. R. Sumner, A. K. Salem, *Biomaterials* **2014**, *35*, 737.

[34] R. M. Raftery, D. P. Walsh, I. M. Castaño, A. Heise, G. P. Duffy, S.-A. Cryan, F. J. O'Brien, *Adv. Mater.* **2016**, DOI 10.1002/adma.201505088.

[35] C. J. Needham, S. R. Shah, R. L. Dahlin, L. A. Kinard, J. Lam, B. M. Watson, S. Lu, F. K. Kasper, A. G. Mikos, *Acta Biomater.* **2014**, *10*, 4103.

[36] J. Y. Park, J.-H. Shim, S.-A. Choi, J. Jang, M. Kim, S. H. Lee, D.-W. Cho, *J. Mater. Chem. B* **2015**, *3*, 5415.

[37] H. C. H. Ko, B. K. Milthorpe, C. D. McFarland, *Eur. Cell. Mater.* **2007**, *14*, 1.

[38] E. J. Sheehy, T. Mesallati, L. Kelly, T. Vinardell, C. T. Buckley, D. J. Kelly, *Biores. Open Access* **2015**, *4*, 229.

[39] O. Jeon, C. Powell, S. M. Ahmed, E. Alsberg, *Tissue Eng. Part A* **2010**, *16*, 2915.

[40]   a I. Van Den Bulcke, B. Bogdanov, N. De Rooze, E. H. Schacht, M. Cornelissen, H. Berghmans, *Biomacromolecules* **2000**, *1*, 31.

[41] W. Lo, A. Tsavaris, D. Peng, M. Eng, H. Lipson, D. Ph, L. J. Bonassar, *Tissue Eng. Part C Methods* **2011**, *17*, 239.

[42] J. Leijten, N. Georgi, L. Moreira Teixeira, C. a van Blitterswijk, J. N. Post, M. Karperien, *Proc. Natl. Acad. Sci.* **2014**, *111*, 13954.

[43] T. Vinardell, E. J. Sheehy, C. T. Buckley, D. J. Kelly, *Tissue Eng. Part A* **2012**, *18*, 1161.

[44] K. P. Egan, T. A. Brennan, R. J. Pignolo, *Histopathology* **2013**, *61*, 1168.

[45] O. Guillaume, S. M. Naqvi, K. Lennon, C. T. Buckley, *J. Biomater. Appl.* **2015**, *29*, 1230.

[46] E. G. Meyer, C. T. Buckley, S. D. Thorpe, D. J. Kelly, *J. Biomech.* **2010**, *43*, 2516.

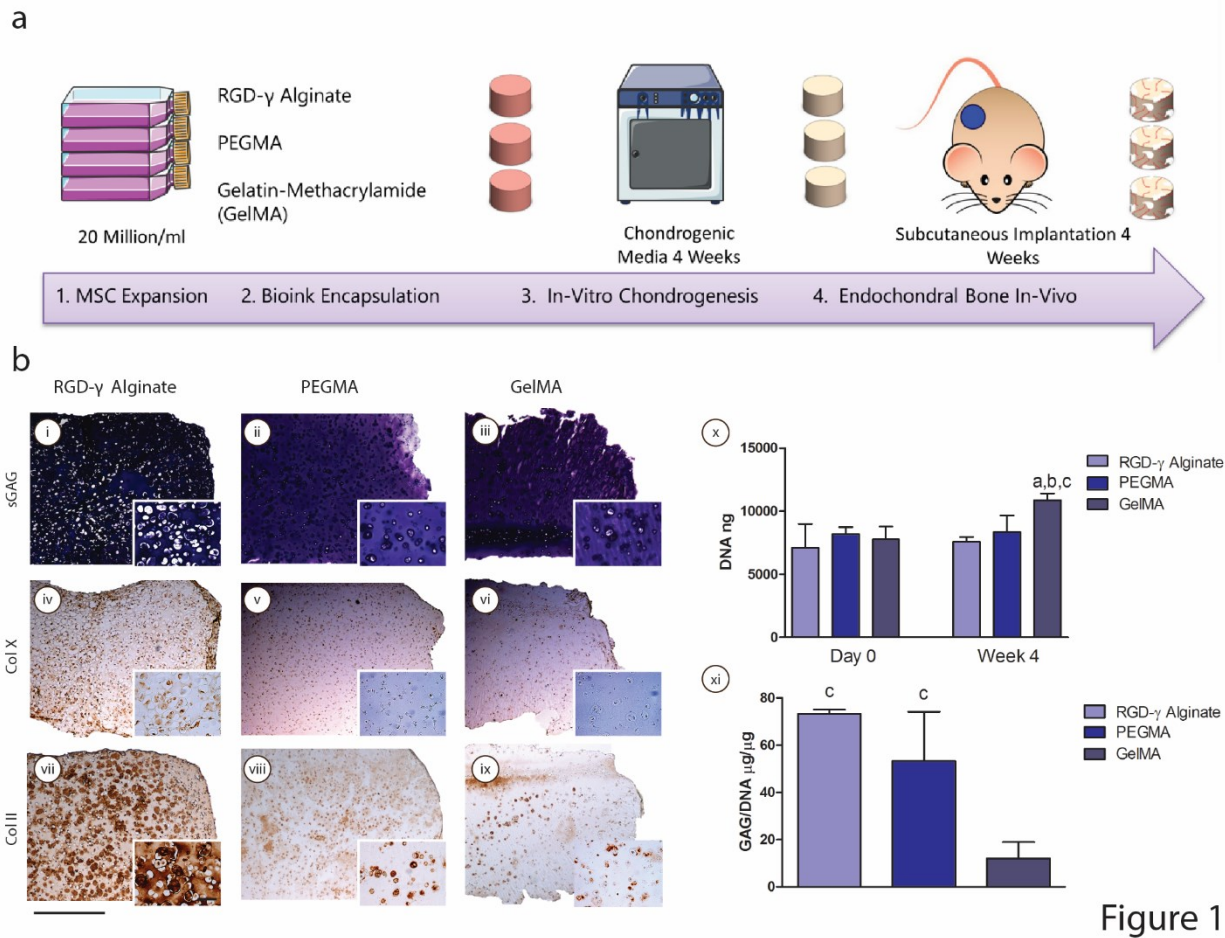[47] T. Mesallati, B. A. Bai, *Eur. Cells Mater.* **2014**, *30*, 163.

Figure 1: Printable Hydrogels for Supporting Chondrogenesis of MSCs. (a) Experimental design: MSCs were encapsulated in each of the hydrogels, chondrogenically primed in vitro and implanted subcutaneously in nude mice. (b) Histological and immunohistochemical analysis of MSC-laden hydrogels following 4 weeks of in vitro culture, (i-iii) aldehyde fuschin/alcian blue (sGAG), immunohistochemical staining for collagen X (iv-vi), collagen type II (vii-ix), biochemical analysis of all hydrogels after 4 weeks of in vitro culture. (x) total DNA content (ng), (xi) sGAG/DNA. (Significance $p<0.05$, ANOVA, Mean $\pm$ SD): (a) vs. RGD-γ alginate at the same time point, (b) vs. PEGMA at the same time point, (c) vs GelMA at same timepoint. 4X throughout along with 20X inset. 4X scale bar 1mm, 20X scale bar 100µm. Staining representative for n=2-3 throughout
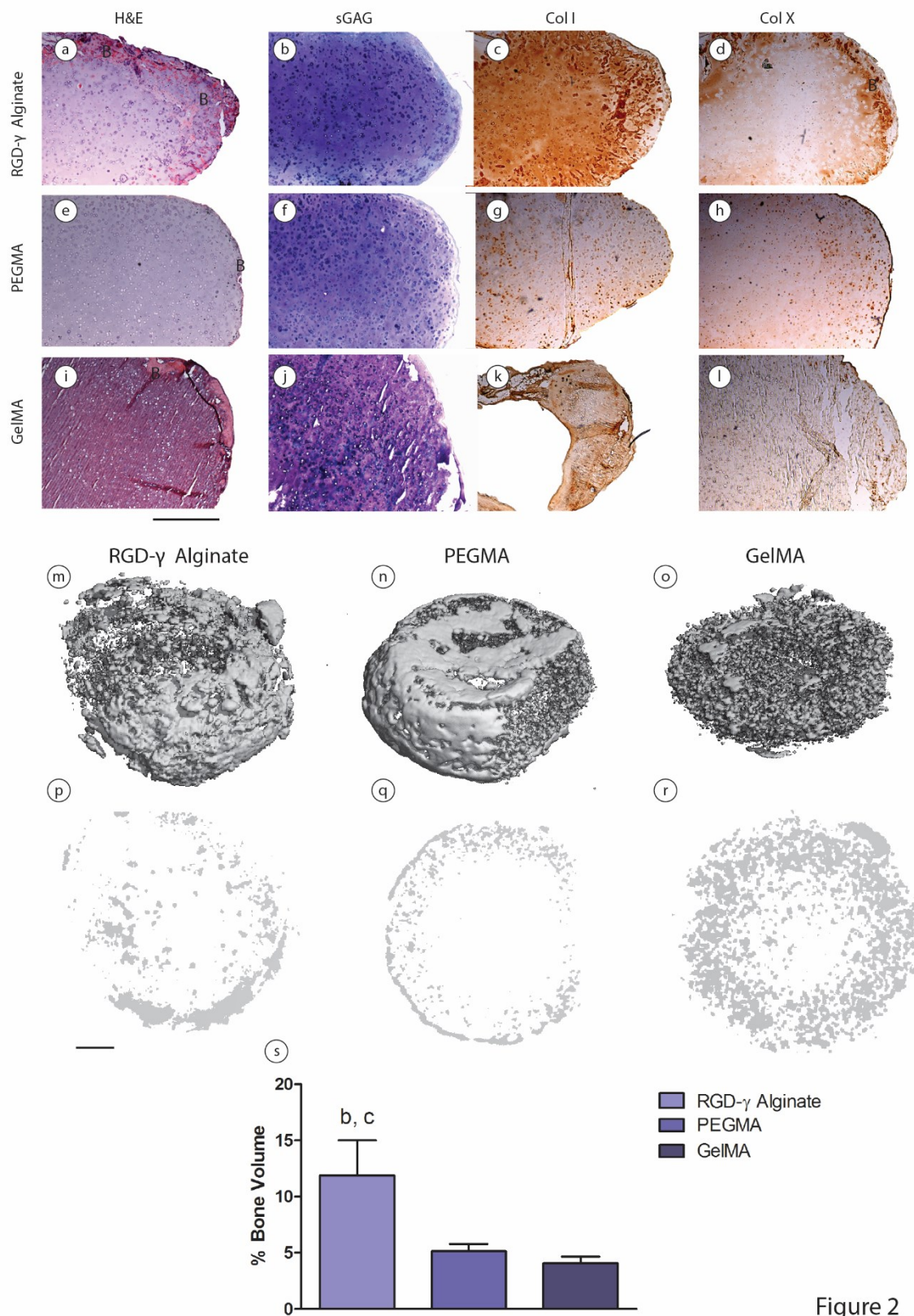
Figure 2

Figure 2: Printable Hydrogels for Endochondral Bone Development In Vivo. μCT, immunohistochemical and histological analysis of hydrogels six weeks post implantation. (a, e, i) H&E staining (darker pink; mineralised bone) for bone formation. (b, f, j) aldehyde fuschin/alcian blue staining for sGAG. (c, g, k) immunostaining for collagen type I. (d, h, l) immunostaining for collagen type X. (m-o) whole μCT reconstruction of hydrogels and (p-r) reconstruction at mid-section. (s) quantification of mineral volume. b, denotes significance vs. PEGMA, c, denotes significance vs. GelMA, (p<0.05, ANOVA, Mean ± SD), scale bar 1mm, B (Bone area). Staining representative for n=3 throughout
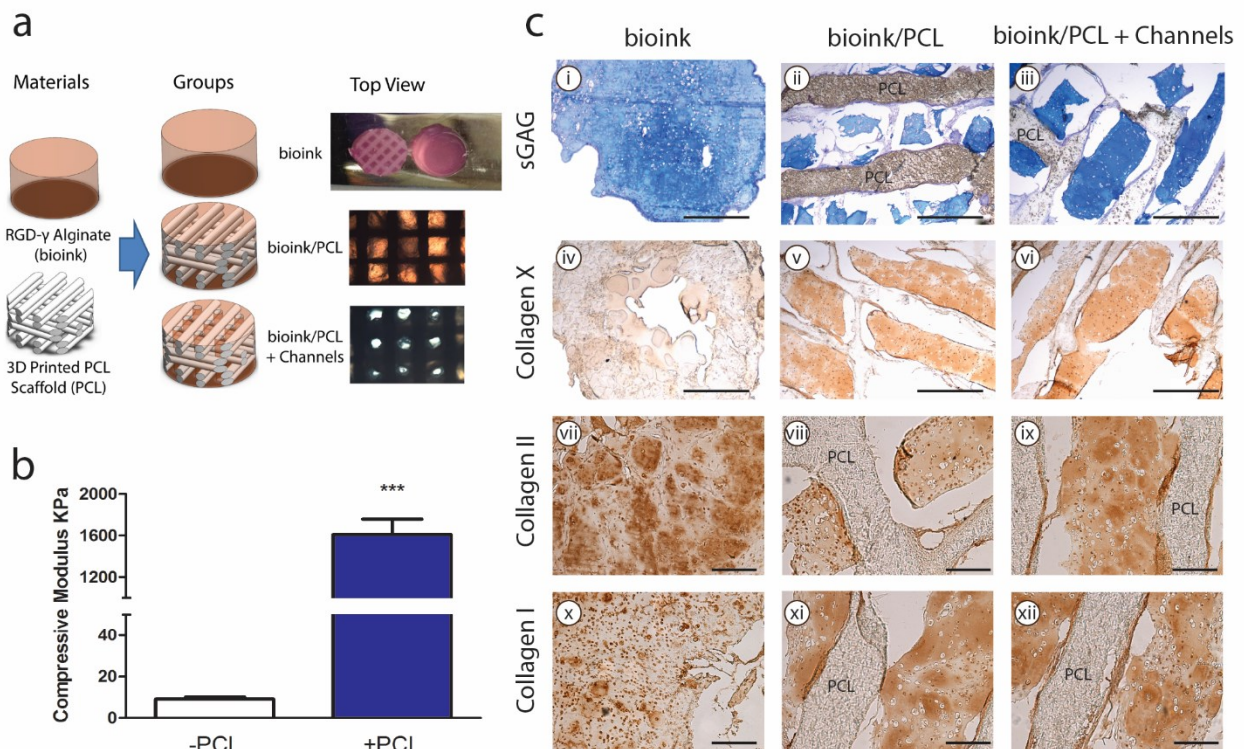
Figure 3

Figure 3 Development of Mechanically Reinforced Bioinks. (a) Study design including description of materials and groups. (b) bioink mechanical properties with and without PCL microfibers. (c) Histology after 4 weeks in vivo, (i-iii) aldehyde fuschin/alcian blue Staining for sGAG, scale bar 1mm, (iv-vi) immunostaining for collagen type X, scale bar 1mm, (vii-ix)

immunostaining for collagen type II, scale bar 400um ,(x-xii) immunostaining for collagen type I, scale bar 400um, (Note for this experiment, the hydrogels were cast into the PCL scaffolds post-printing).
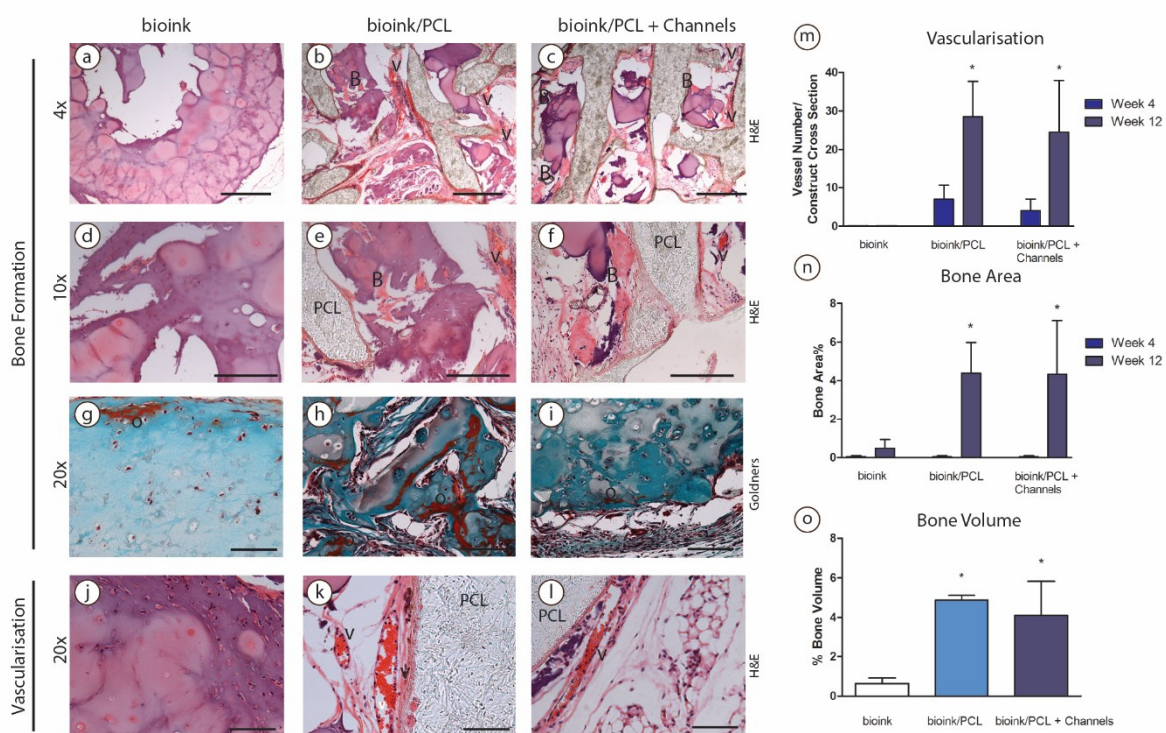

Figure 4

Figure 4: Mechanically Reinforced Bioinks Support Endochondral Bone Formation in Vivo. H&E staining of all groups after 12 weeks post-implantation (a-c) 4x scale bar 1mm (d-f) 10x scale bar 500um. (g-l) Goldners trichrome staining for bone, 20x scale bar 100um, red regions indicate unmineralized osteoid tissue. (m) Histomorphometric quantification of bone area at construct mid and quarter section after 4 and 12 weeks in vivo, *denotes significance ($p < 0.05$, ANOVA, Mean ± SD) compared to bioink group at same timepoint (4/12 weeks). (n) Histomorphometric quantification of areas of blood vessel activity at construct mid and quarter section after 4 and 12 weeks in vivo,

*denotes significance ($p < 0.05$, ANOVA, Mean ± SD) compared to bioink group at same timepoint (4/12 weeks). (o) Quantification of mineral volume by μCT after 12 weeks in vivo, *denotes significance ($p < 0.05$, ANOVA, Mean ± SD) compared to bioink. B (Bone formation), V (Vessel Formation), O (Osteoid). (Note for this experiment, the hydrogels were cast into the PCL scaffolds post-printing).
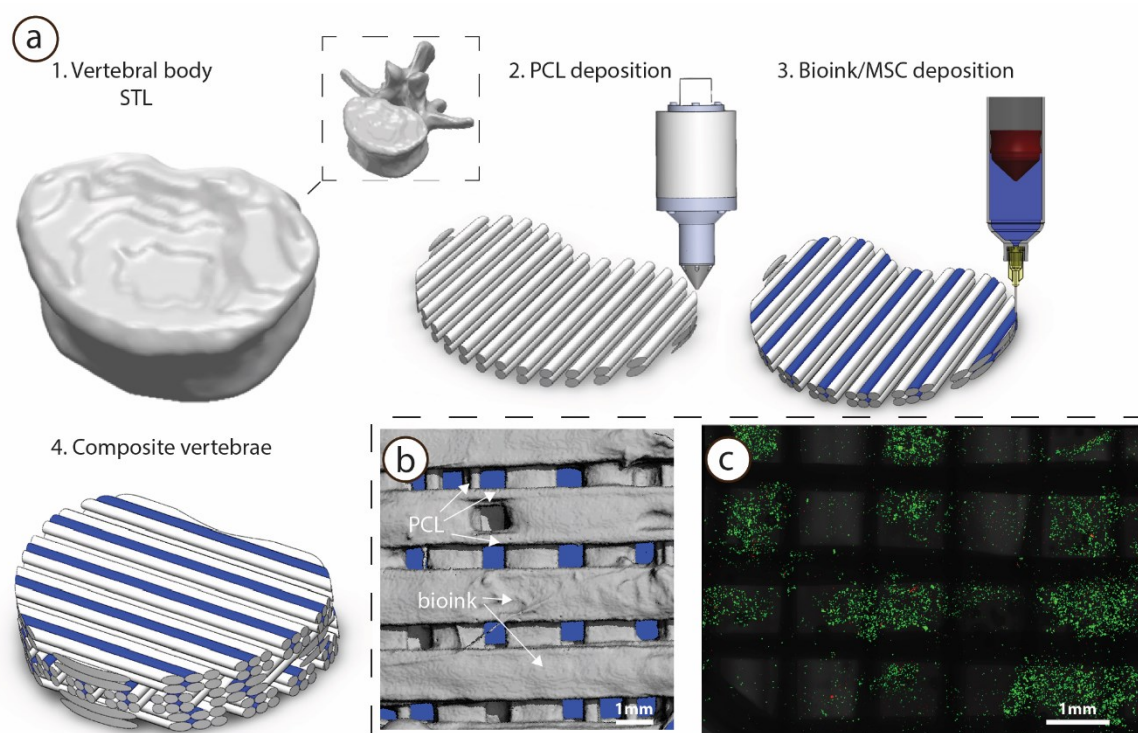

Figure 5

Figure 5 3D Bioprinting of Vertebrae Shaped Mechanically Reinforced Bioinks. (a) Description of multi-tool 3d bioprinting process, 1) The outer geometry of a human vertebral body was scanned and next layers of 2) PCL filaments were deposited followed by deposition of the 3) MSC laden

26

bioink, this was repeated in an orthogonal fashion to create a 4) composite vertebrae structure. (b) µCT analysis demonstrated the distribution of bioink and PCL within the composite vertebrae. Bioink + PCL filaments isolated using µCT, indicating the presence of bioink free channels conduits (blue regions) post-printing. (c) Live dead images of cells within the deposited bioink 1 hour post-printing, scale bar 1mm
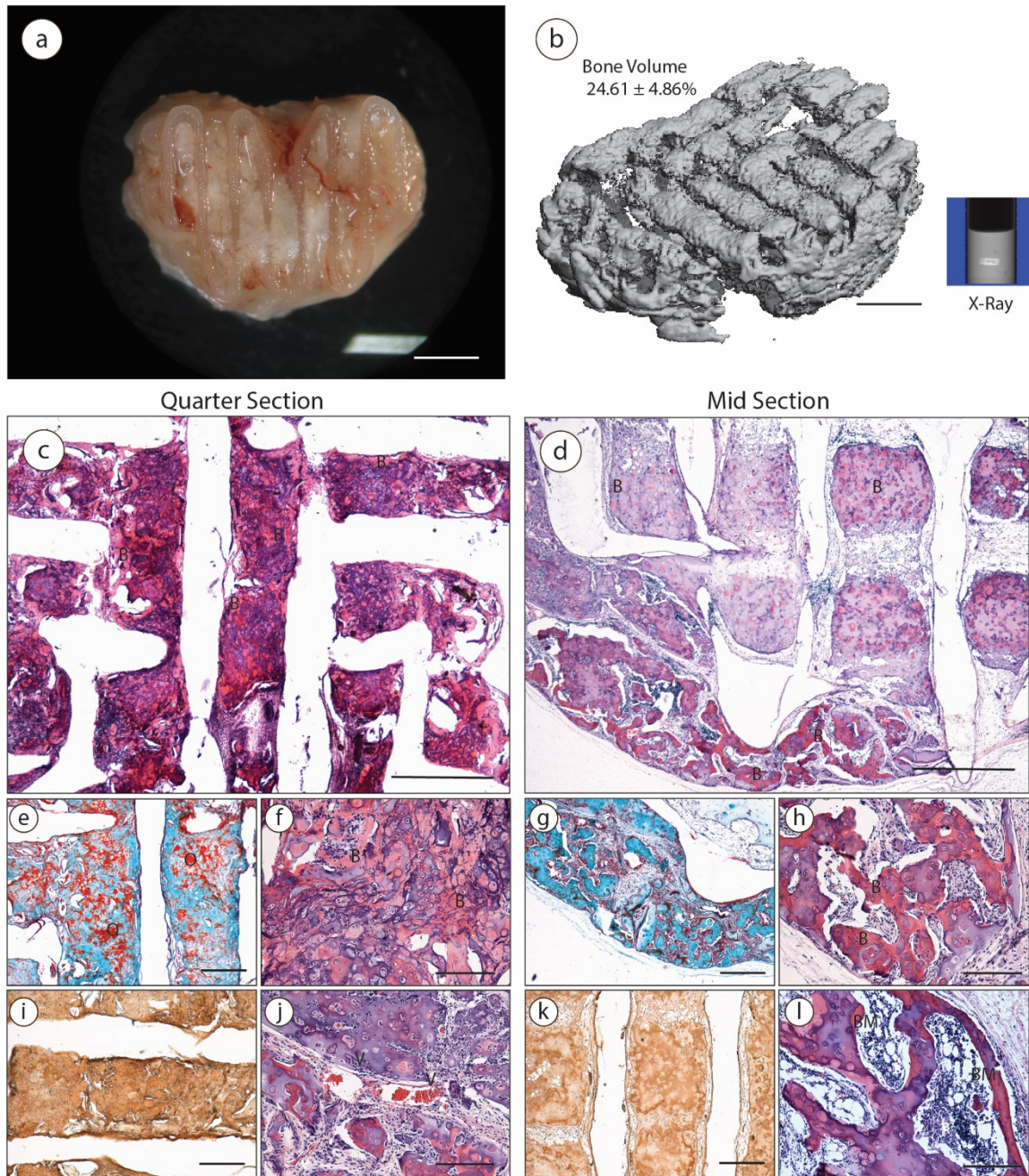
Figure 6 Development of Vascularised Bone Organ In Vivo Following implantation of Cartilage Rudiment. (a) Macroscopic image of anatomically shaped vertebrae constructs 12 weeks post-implantation scale bar 2mm. (b) μCT reconstruction and x-ray of whole construct, scale bar 2mm. (c, d) H&E staining of construct at quarter and mid sections, 2X scale bar 1mm. (e, g) goldners trichrome staining of construct, (red; non-mineralised bone, green; mineralised bone, 4X scale bar 400μm. (i, k) collagen type X staining, 4x scale bar 400μm. (f, h, j l) H&E staining, 10X scale bar 200 μm. (B) Bone, O (Osteoid), V (Blood Vessel), BM (Bone marrow like tissue).

TOC Entry:

A novel biofabrication strategy is described where 3D bioprinting is used to engineer the developmental precursor to an adult organ. These bioprinted cartilage templates have the capacity to mature into vascularised bone organs *in vivo.* It was possible to reinforce these immature cartilage pre-cursors with polycaprolactone (PCL) micro-fibres, providing a level of mechanical functionality compatible with implanting such immature organ rudiments into load bearing locations *in vivo.*
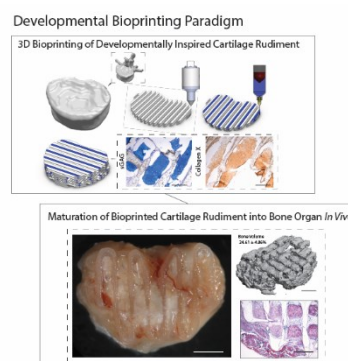
Supporting Information

3D Bioprinting of Developmentally Inspired Templates for Whole Bone Organ Engineering

Andrew C. Daly, Gráinne M. Cunniffe, Binulal N. Sathy, Oju Jeon, Eben Alsberg, Daniel J. Kelly,
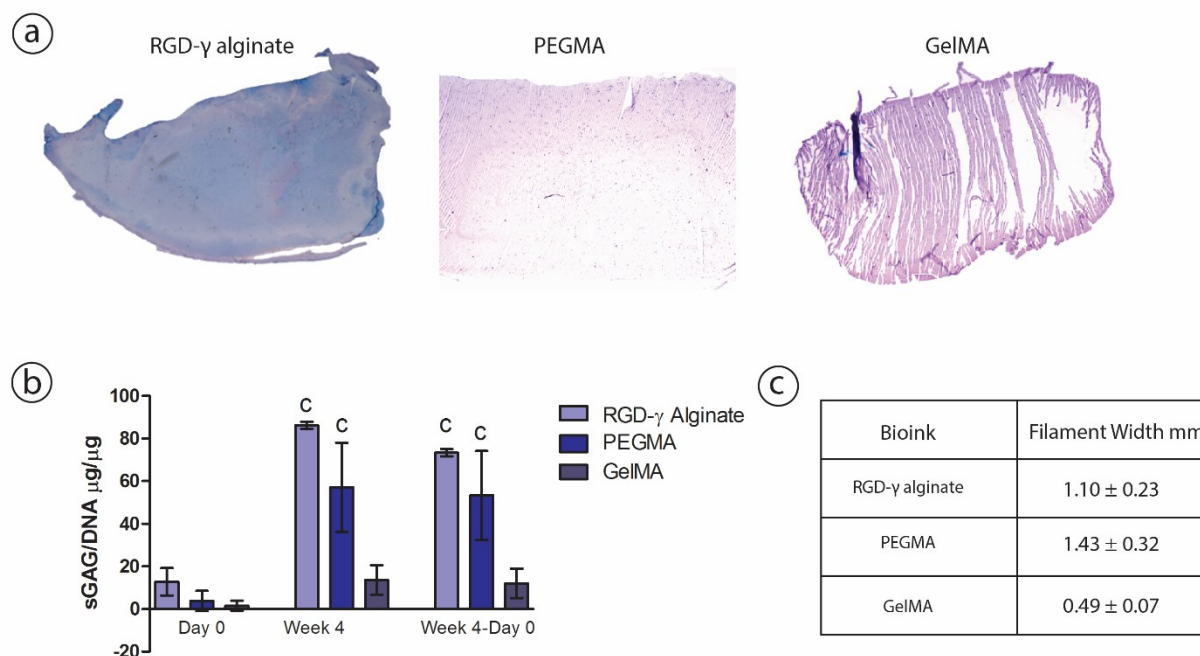
Supplementary Figure S1: Printable Hydrogels for MSC Chondrogenesis (Study 1). (A) Acellular Aldehyde fuschin/alcian blue staining for each hydrogel. (B) Day 0 and week 4 sGAG values for each hydrogel before and after four weeks in chondrogenic culture conditions. (C) Average filament width for each bioink for comparison of bioink printability (Mean ± SD, n=4).
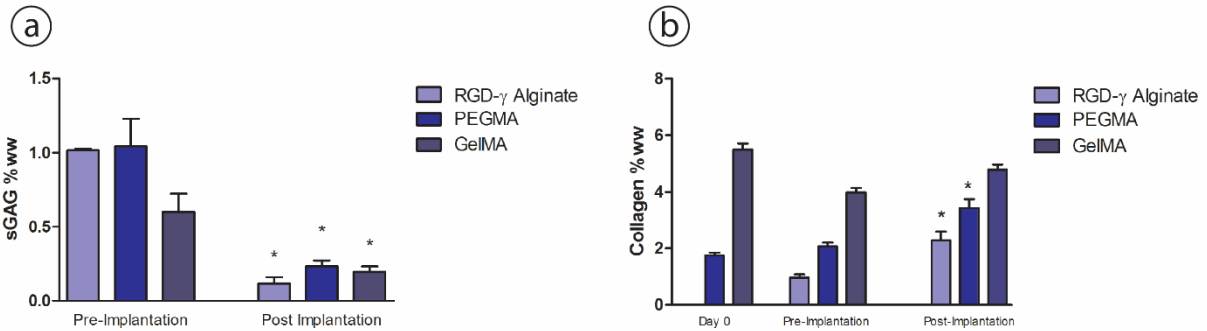
Supplementary Figure S2: Quantification of sGAG and collagen production pre and post implantation (Study 1). (a) sGAG %ww content pre-implantation (after 4 weeks in chondrogenic conditions) and post-implantation (followed by 6 weeks of subcutaneous implantation *in vivo*). (b) Collagen %ww content day 0, pre-implantation and post-implantation (Note the levels of collagen at day 0 are due to the presence of collagen in the commercially available PEGMA bioink and interaction of the hydrolysed collagen (Gelatin) with the hydroxyproline assay) .* denotes significance between pre and post implantation protein levels within same hydrogel, ($p<0.05$, ANOVA, Mean ± SD).
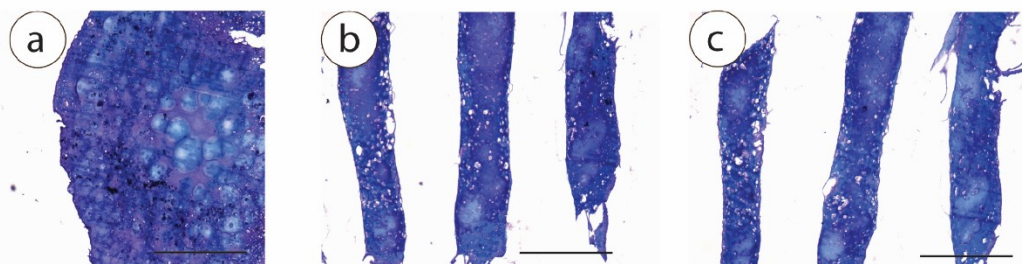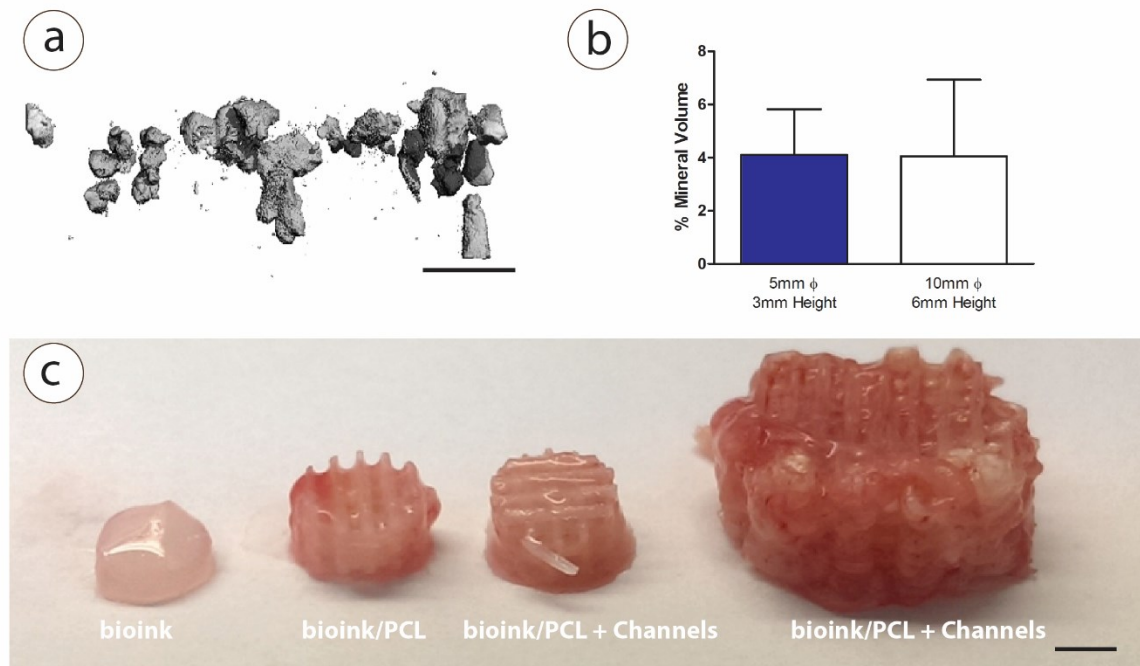

Supplementary Figure 1

Supplementary Figure S3: Composite Bioinks pre-implantation (Study 2). Aldehyde fuschin/alcian blue staining pre implantation confirming the presence of sGAG and chondrogenic

differentiation (a) bioink, (b) bioink/PCL, (c) bioink/PCL + channels (note channels had not been introduced at this stage) scale bar 1mm

Supplementary Figure 2

Supplementary Figure S4: Scalability of Process (a) uCT reconstruction of larger (10mm Ø X 6mm height) bioink/PCL + channels 12 weeks post-implantation. Scale bar 2mm (b) Comparison of mineral volume present in smaller (5mm Ø X 3mm height bioink/PCL + channels) and larger (10mm Ø X 6mm height bioink/PCL + channels) constructs post implantation (ANOVA, P<0.05 Mean ±SD) (c) Macroscopic images of all constructs, (bioink, bioink/PCL, small bioink/PCL + channels and large bioink/PCL + channels 12 weeks post implantation, scale bar 2mm

Supplementary Figure 3
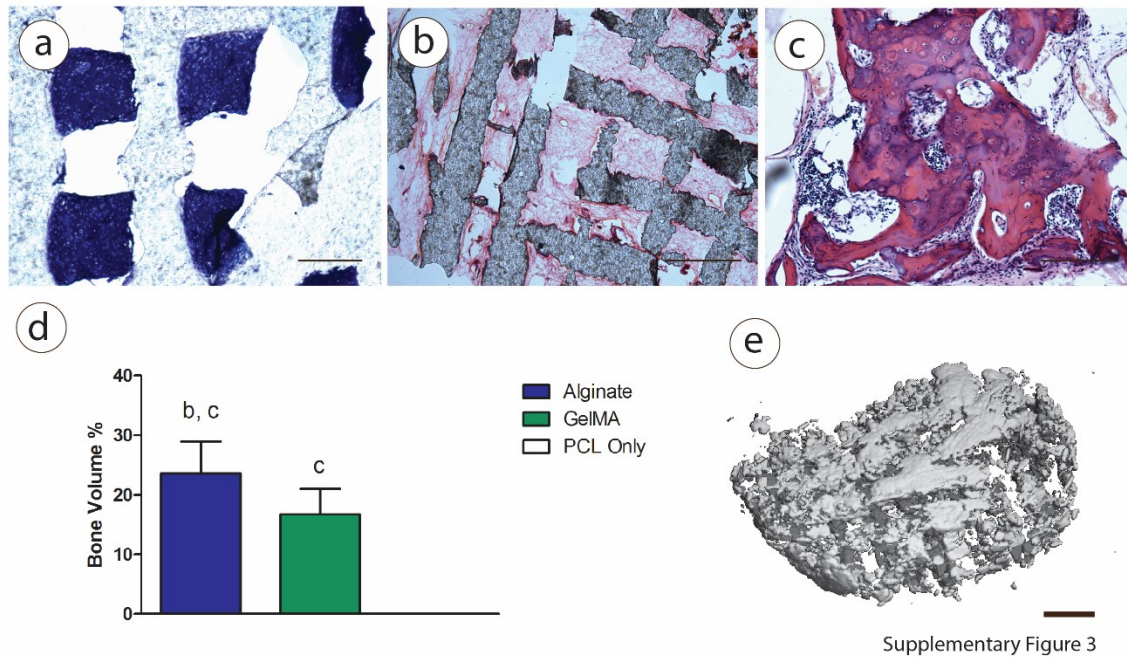
Supplementary Figure S5: Tissue Engineered Vertebrae Controls (a) Aldehyde fuschin/alcian blue staining pre implantation confirming the presence of sGAG and chondrogenic differentiation within vertebrae structure (b) H&E staining of empty PCL vertebrae filled with fibrous fatty tissue 12 weeks post implantation, scale 1mm. (c) H&E staining confirming the presence of bone within vertebrae engineered using a GelMA bioink, scale 200µm (d) µCT quantification of mineralisation within vertebrae engineered using RGD-γ alginate & GelMA bioinks and with empty (bioink/MSC free) PCL vertebrae control, *denotes significance (p<0.05, one way ANOVA, Mean ± SD) compared to PCL only (e) µCT reconstruction of mineralisation within Vertebrae engineered using GelMA bioink